Electronic and vibrational properties of the two-dimensional Mott insulator $V_{0.9}PS_3$ under pressure

Matthew John Coak,[1,2,3,*] Yong-Hyun Kim,[4] Yoo Soo Yi,[5] Suhan Son,[1,2] Sung Keun Lee,[4] and Je-Geun Park[1,2]

[1]*Center for Correlated Electron Systems, Institute for Basic Science, Seoul 08826, Republic of Korea*

[2]*Department of Physics and Astronomy, Seoul National University, Seoul 08826, Republic of Korea*

[3]*Department of Physics, University of Warwick, Gibbet Hill Road, Coventry CV4 7AL, United Kingdom*

[4]*School of Earth and Environmental Science, Seoul National University, Seoul 08826, Republic of Korea*

[5]*Korea Polar Research Institute, 26 Songdomirae-ro, Incheon 21900, Republic of Korea*

(Received 30 May 2019; revised manuscript received 1 July 2019; published 19 July 2019)

We present a Raman spectroscopic study of the layered antiferromagnetic Mott insulator $V_{0.9}PS_3$ and demonstrate the evolution of the spectra with applied quasihydrostatic pressure. Clear features in the spectra are seen at the pressures identified as corresponding to a structural transition between 20 and 80 kbar and the insulator-metal transition at 120 kbar. The feature at 120 kbar can be understood as a stiffening of interplanar vibrations, linking the metallization to a crossover from two- to three-dimensionality. Theoretical *ab initio* calculations, using the previously determined high-pressure structures, were able to reproduce the measured spectra and map each peak to specific vibration modes. We additionally show calculations of the high-pressure band structure in these materials, where the opening of a band gap with an included Hubbard U term and its subsequent closing with pressure are clearly demonstrated. This little-studied material shows great promise as a model system for the fundamental study of low-dimensional magnetism and Mott physics.

DOI: 10.1103/PhysRevB.100.035120

I. INTRODUCTION

Low-dimensional materials, especially the two-dimensional (2D) case of layered structures separated by weak van der Waals gaps, have long provided robust test beds for investigating fundamental physics but are now enjoying a surge of interest for both device applications and magnetism research [1–5]. For device applications and the physics of nanostructures and heterostructure assemblies it would be very useful to command the ability to easily and cleanly select the material thickness down to single layers, as well as to have fine control over both novel magnetic states and tunable electronic band gaps in semiconducting systems. Fundamental questions about the nature of truly 2D magnetic order and the emergence of metallic or superconducting states from antiferromagnetic Mott-insulating phases can also be answered in these simple, clean, controllable systems.

One particularly rich, and long overlooked, family of materials now under intense scrutiny worldwide is MPX_3, where M denotes a first-row transition metal and X either S or Se. First synthesized by Klingen in 1969 [6–8] and later reviewed comprehensively by Grasso and Silipigni [9], they have been studied in detail in more recent years as excellent examples of 2D magnetic systems. The MPX_3 compounds form a layered honeycomb lattice of the metal ions [10–13] with monoclinic space group $C2/m$ and interplanar forces solely through a van der Waals interaction between P_2S_6 clusters surrounding the metal ions. They can be easily mechanically exfoliated as with graphene and have been shown to maintain their magnetic ordering down to monolayer thickness [14,15], while also allowing easy and clean assembly of complex heterostructures of different functional van der Waals materials. While the material family is mainly isostructural, electronic band gaps, spin states, magnetic ordering, magnetic anisotropy, and critical behavior change with the choice of transition metal [16–25].

MPX_3 compounds all show insulating, exponentially increasing resistivity with decreasing temperature—and can be described as p-type semiconductors [9] and as Mott insulators [26,27]. Recent works have demonstrated Mott insulator–metal transitions in $MnPS_3$, $FePS_3$, and $V_{0.9}PS_3$ [26–29] and, additionally, superconductivity in $FePSe_3$ [30]. Historically, the calculation of realistic band structures for these materials has proved challenging, and only recently have precise theoretical works begun to emerge [31]. Theoretical understanding of the high-pressure metallic states and of the evolution of the systems as they approach metallization is a crucial ingredient in advancing our understanding of this physics. van der Waals compounds such as these are perfectly suited to high-pressure studies, where the hydrostatic pressure has the predominant effect of smoothly and controllably reducing the interlayer spacing and hence moving towards three-dimensionality, while avoiding complications of doping or disorder.

$V_{1-x}PS_3$, with x the level of vanadium deficiency, is an MPX_3 compound that has been long overlooked despite its great potential, with only a few basic properties characterized. It has the smallest band gap of the MPX_3 compounds at around 0.25 eV [12,32,33] and by far the lowest resistivity (of the order of Ω cm) at room temperature—suggesting that it could be useful as an ingredient in van der Waals transistors and other devices. This can additionally be tuned over an order of magnitude by altering the level of vanadium deficiency [33]. Our earlier study [27] reported on the high-pressure structure and the anomalous transport behavior of

*matthew.coak@warwick.ac.uk

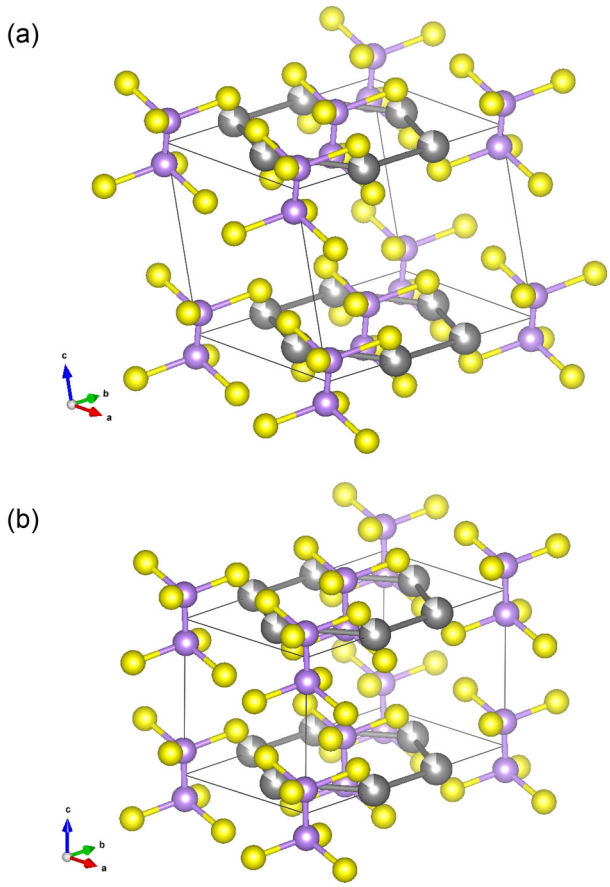

FIG. 1. Crystal structures and parameters of the high- and low-pressure phases of $V_{0.9}PS_3$, taken from [27]. Crystal structure of $V_{0.9}PS_3$ (a) at 11 kbar, the LP phase, and (b) at 177 kbar, the HP-I phase. The HP-I structure has β close to 90° so atoms in each plane are aligned with their equivalents in neighboring planes.

this material and uncovered a gradual structural transition between 20 and 80 kbar (Fig. 1), followed by an insulator-metal transition around 120 kbar. The resistivity was reported in this work as the 1D (or equivalent) variable-range-hopping type, rather than Arrhenius in this compound, so the band-gap value extracted from the resistivity fits in the literature is not a precise indication of a true gap. The dimensionality of the transport was intriguingly shown to tune from 1D up to 3D at the point of metallization.

Like most members of the MPX_3 family, $V_{1-x}PS_3$ is antiferromagnetic [12], with a Néel temperature of around 62 K, but to date there has been no detailed study of its magnetic structure. We can infer from the vanadium deficiency in $V_{1-x}PS_3$ that there is most likely valence mixing at the vanadium site between V^{2+} and V^{3+} states. An interesting parallel can then be drawn to $VAgP_2S_6$ [34], where the mixture of V^{3+} ($S = 1$) and Ag^{1+} ions on the honeycomb lattice leads to long-range ordering of these sites into 1D chains and the emergence of a Haldane-gapped spin-chain state.

II. METHODS

Single crystals of $V_{0.9}PS_3$ were grown via a chemical vapor transport method in a two-zone tube furnace at temperatures of 600 and 350 °C for 1 month using 0.1 g of $TeCl_4$ flux for 1 g of reactants. Prior to the reaction, the quartz tubes used were cleaned and dried, loaded with V (99.5%), P (99.99%), and S (99.98%) powders under an argon atmosphere, then evacuated to 5×10^{-3} mbar with an oil diffusion pump before sealing. The crystals form with vanadium deficiency, due to its natural tendency to V^{3+} valence (the transition metal in MPX_3 is M^{2+}), so a 20% excess of vanadium powder was added to the reactant mixture to attempt to mitigate it. Crystals were characterized by powder and single-crystal diffraction for phase purity and by energy-dispersive x-ray spectroscopy for stoichiometry. The samples used in this study had a stoichiometry of $V_{0.9}PS_3$, with an uncertainty of ± 0.05 on the 0.9 vanadium fraction, and were from the same batch reported in our recent transport and structural study [27].

For Raman spectroscopy measurements, several single crystals of $V_{0.9}PS_3$ were ground into a fine powder in an argon atmosphere glove box, while immersed in liquid nitrogen; the cryogenic grinding makes the material more brittle and helps mitigate preferred orientation of the crystallites. This powder was packed into the sample region of a diamond anvil cell [35,36] with 400-μm diamond culets and a stainless-steel gasket with a 140-μm sample space hole. A powder sample ensures that all Raman peaks will be captured, as there should be no directional dependence, and allows a large filling factor of the sample region. No pressure medium was used; preliminary tests with glycerol and methanol-ethanol mixtures showed peaks from the pressure medium overwhelming the sample signal, and our previous structural studies on this family of compounds [26] have shown that, due to the softness of these materials, there is little difference between data collected with even a helium pressure medium and data collected with no medium. The pressure values were measured through the fluorescence of miniature ruby spheres included in the pressure region [37]. Due to the quasihydrostatic nature of the pressure, particularly at higher pressures, pressure gradients up to 15% could be measured, depending on the ruby position within the sample region. The pressure was taken as the maximum value measured for each point, and so true pressures could potentially be slightly lower than reported here.

The Raman spectra were collected at room temperature on a micro-Raman spectrometer with a 488-nm Ar-ion laser and a grating groove density of 1800 L mm^{-1}. The collection time was 2 s and each spectrum was accumulated 300, 600, or 900 times depending on the overall signal/noise ratio. The overall spectral resolution is ~0.55–0.85 cm^{-1}/pixel and the spectrometer slit width 100 μm. All spectra were collected with 20× microscope objectives. A separately collected background spectrum was subtracted from the data, and a general polynomial background was additionally subtracted and the data normalized to the highest peak.

The theoretical calculations were carried out in CASTEP [38], using the low- and high-pressure structures found in our earlier study [27]. The on-site electron-electron interactions were determined with the generalized gradient approximation (GGA)–based Perdew-Berke-Ernzerhof (PBE) exchange-correlation functional [39]. Long-range interactions such as the van der Waals interaction are significant for layered

structures like $V_{0.9}PS_3$ so a hybrid semiempirical dispersion correction term based on the Tkatchenko-Scheffler method was applied during the calculations [40]. The interatomic interactions among atoms were represented with the norm-conserving on-the-fly pseudopotential [38]. The plane-wave cutoff energies, used to define the precision of the electronic wave functions, were set to 1000 eV. The convergence criterion for the self-consistent field calculations for the structure optimization was set to 10^{-6} eV/atom. The Monkhorst-Pack grid was set to $7\times7\times1$ to define the k points (i.e., 16 irreducible k points and the Γ point included). The convergences of the plane-wave cutoff energy and the Monkhorst-Pack grid for k points were tested; there were no significant differences when using higher precisions. Initial structure optimizations were performed to refine the crystal structures beyond the experimental precision of x-ray diffraction for the vibrational frequency calculations. The Broyden-Fletcher-Goldfarb-Shanno (BFGS) algorithm [41] was used for the geometry optimization algorithm. The convergence criteria of the structure optimization were set to 10^{-5} eV/atom, 0.03 eV/Å, 0.05 GPa, and 0.001 Å for the total energy, maximum forces, maximum stress, and maximum displacement, respectively. This then allowed the simulated IR and Raman spectra to be calculated. The finite displacement method was used to obtain the Raman intensity [42,43]. The band structures and partial density of states were calculated more precisely. The GGA + U method [44], including the effects of spin polarization, was used, with Hubbard U values from 0.0 to 4.5 eV investigated. Previous studies have used values in the range 3.0–3.5 eV [45–47] for vanadium ions, lower than the 4.0–4.5 eV used for iron [48,49]. We present results using a U of 3 eV as well as their equivalents if the much smaller 1-eV value is used.

III. RESULTS

The Raman spectra for $V_{0.9}PS_3$ at room temperature are shown for pressures ranging from 0 to 240 kbar (24 GPa) in Fig. 2. The ambient pressure data show an equivalent arrangement of peaks to those reported in isostructural compound $FePS_3$ by Lee *et al.* [14] and extensively mapped to specific vibrational modes—with comparable peak shapes and broadness. All MPS_3 materials investigated so far (Mn, Ni, Fe, V) have displayed the same structural transitions between the LP, HP-I, and HP-II phases outlined by Haines *et al.* [26] in $FePS_3$; the evolution of Raman peaks in this vanadium compound is likely to be universal in character across the whole family. It should be noted that due to the finite crystallite size in the powder used and the strong effects of preferred orientation, the relative heights of peaks in the spectra are not reliable—but their evolution is physical, as the same area of the sample was used throughout. We call the peaks p1, p2, p3, and p4 for ease of reference as shown by arrows in Fig. 2.

Figure 3 shows the pressure evolution of each peak position. All peaks shift upwards in energy/wave number as the pressure is increased, consistent with the gradual decrease in the lattice parameters. As shown in our structural study [27], there are no abrupt changes in unit cell volume up to the maximum pressure investigated therein (177 kbar), and correspondingly there are no jumps in Raman mode energies. The p3 peak can be seen to be gradually suppressed in Fig. 2, completely disappearing between 80 and 100 kbar. This is consistent with the earlier structural results, which showed a gradual crossover from the LP low-pressure phase to the HP-I phase between 20 and 80 kbar; above 80 kbar there should be no remaining phase fraction of the LP phase and hence the p3 peak (therefore assumed to be unique to this phase) is lost or moved into the same energy as the p2 peak.

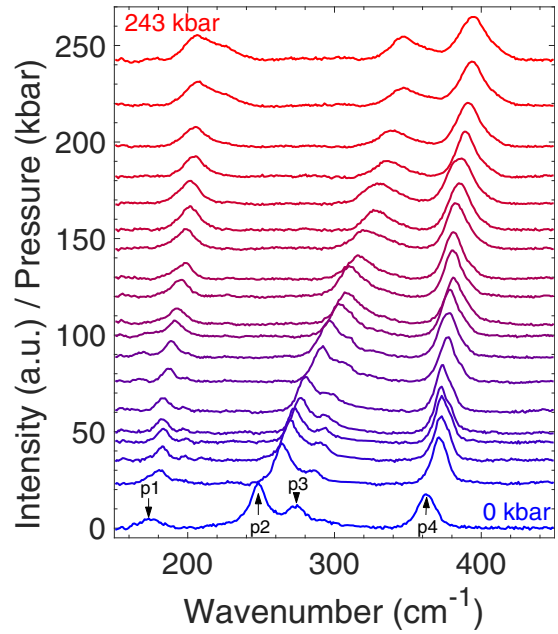

FIG. 2. Normalized Raman intensities for powder $V_{0.9}PS_3$ taken at room temperature at increasing pressures. The y intercept of each data set has been set to its corresponding pressure value. Four peaks, labeled with arrows, can be identified at ambient pressure. Peak p3 is gradually suppressed and disappears around 90 kbar.

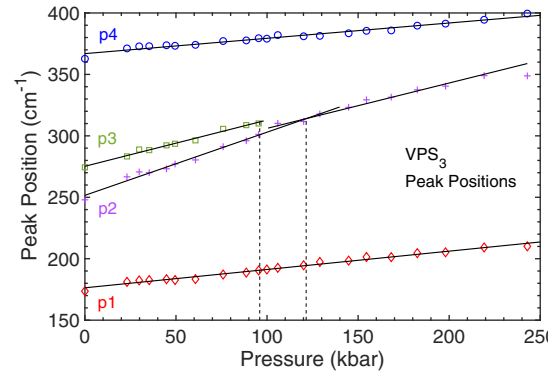

FIG. 3. Raman peak positions for powder $V_{0.9}PS_3$ taken at room temperature at increasing pressures, extracted from fits to Fig. 2. All peaks shift upwards in wave number as the pressure is increased, in line with lattice compression, but peak p3 vanishes around 90 kbar and a change of slope in the pressure dependence of peak p2 is evident at around 120 kbar. The equations of the fits are as follows (pressures in kbar, peak positions in cm^{-1}): p1, $0.149p + 176.3$; p2, $0.514p + 251.6$ and, at high pressure, $0.369p + 269.2$; p3, $0.376p + 275.2$; and p4, $0.125p + 366.9$.

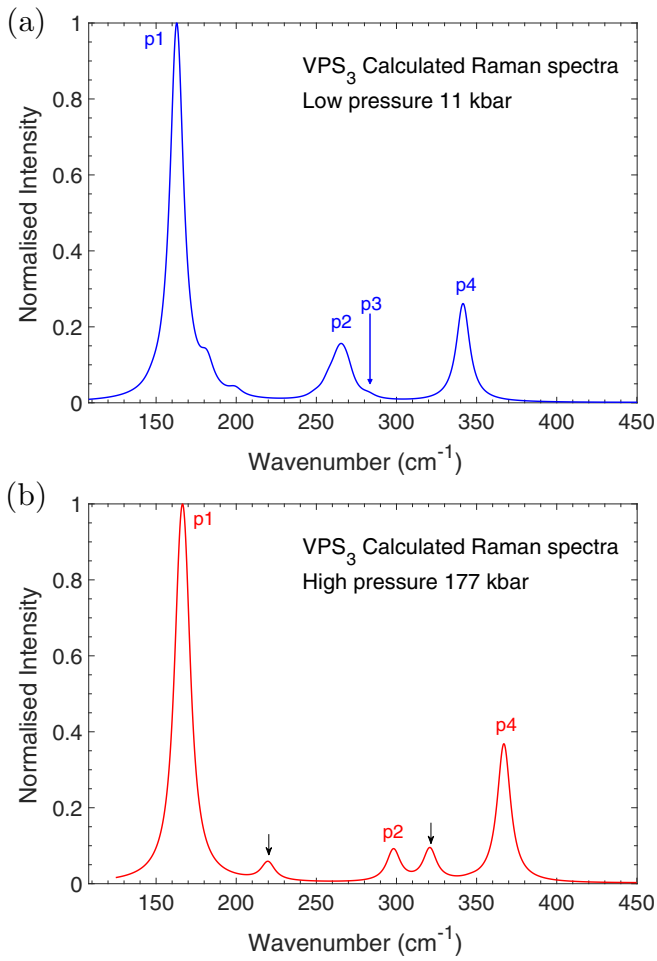

FIG. 4. Calculated Raman spectra for $V_{0.9}PS_3$ at (a) 11 kbar and (b) 177 kbar, using the structural information from [27]. The peaks can be matched to those shown in Fig. 2, as annotated, except for two small peaks in the high-pressure phase, marked with unlabeled black arrows. The preferred orientation and imperfect powder averaging mean that the experimental and theoretical peak heights will not agree.

An additional feature of interest is the pressure dependence of the p2 peak. Unlike the other peaks, which show a good agreement with linear fits, the behavior of p2 was best described by two separate linear slopes at low and at high pressures, with a kink or change in slope around 120 kbar (an uncertainty of around 10 kbar results from the high sensitivity of such a line crossing to different fit regimes) from 0.514 to 0.369 cm^{-1}/kbar. This pressure range corresponds to the metallization pressure previously reported, along with the crossover to 3D transport. The reduced slope at this kink corresponds to a stiffening of the mode—the mode energy is altered less by compression of the lattice than it was in the insulating state—and again there is no visible change in the other modes. All of this behavior is consistent with an insulator-metal transition associated with gradually increased electron overlap between crystal planes.

Using the room-temperature structural information obtained in our previous work [27] at the Diamond Light Source, we were able to calculate the simulated Raman spectra at the lowest and highest pressures measured in the structural study, 11 and 177 kbar. Eleven kilobars is well within the purely LP phase and corresponds to the ambient-pressure structure, while 177 kbar is deep into the HP-I phase and above the metallization pressure. These simulated spectra are plotted in Fig 4. As mentioned in the previous section, peak heights in the experimental data will have been heavily modulated by preferred orientation effects; disregarding this difference, we can see a good correspondence between the calculated and the experimental spectra. Peaks p1, p2, p3, and p4 can be clearly identified and assigned to modes at the correct energies, and hence the underlying vibrational modes for each peak visualized. Two peaks in the high-pressure simulation plotted in Fig. 4 are not visible in the experimental data, but this may be, again, a result of the preferred orientation

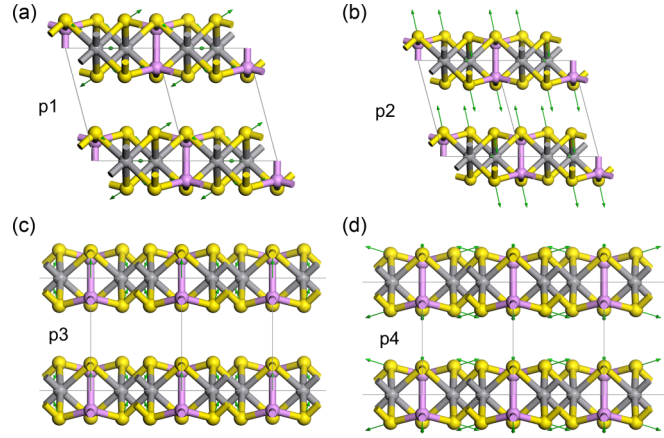

FIG. 5. Visualizations, looking along the *ab* planes, with unit cell boundaries shown in light gray, from calculation of Raman vibrational modes: (a) p1, (b) p2, (c) p3, and (d) p4 at 11 kbar. Mode p2 stands out as being an out-of-plane motion along the c^* axis.

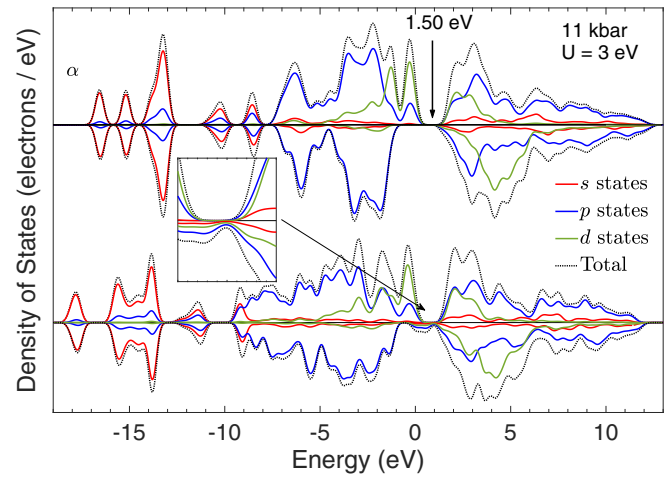

FIG. 6. Calculated partial and total spin-polarized densities of states for $V_{0.9}PS_3$ at 11 and 177 kbar, using structural information from [27]. These are calculated using a Hubbard U of 3 eV for the vanadium on-site repulsion. Reducing this quickly closes the ambient pressure band gap. Inset: Zoomed-in view of the closed gap region from 0 to 2 eV.

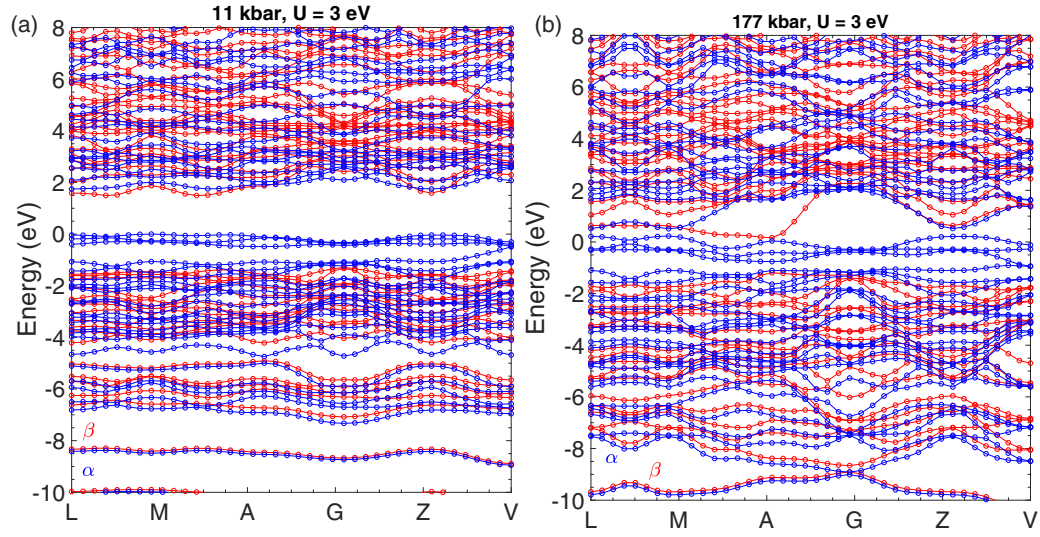

FIG. 7. Calculated spin-polarized band structures (up spin states in blue and down spin states in red) of $V_{0.9}PS_3$ with a Hubbard U of 3 eV (a) at 11 kbar (band gap of 1.495 eV) and (b) at 177 kbar.

suppressing peak intensities, as was found to be the case in x-ray studies.

Additionally, the prediction of vibrational modes for metallic systems like this using *ab initio* methods can introduce certain uncertainties due to the difficulties in defining the Hessian matrix from calculated electronic structures. CASTEP only supports the calculation of electronic structures in the absence of U when calculating the vibrational modes. Therefore, the calculated electronic structures of metallic $V_{0.9}PS_3$ may deviate from the true electronic features or those calculated with the Coulomb interaction included. The shifting of all modes to higher energies along with lattice compression was well reproduced in the calculation.

Visualizations of each of the phonon modes in the LP phase are displayed in Fig. 5. Mode p2 starkly stands out in contrast to the complex in-plane twisting and breathing of the other modes; p2 corresponds to interplanar motion almost purely along the c^* axis. This is the mode which appears to stiffen at the metallization pressure, whereas the others are unaffected. That its interplanar nature makes it uniquely affected by the transition is then fully consistent with the transport properties being explained as a gradual tuning from 2D to 3D, with eventual insulator-metal crossover when interplanar interactions reach a threshold level. Mode p3, which is suppressed as the system moves into the near-trigonal HP-I phase (with $\beta \simeq 90^\circ$), can be understood as an in-plane rotation of the P_2S_6 molecular clusters. These are responsible for mediating the interplanar interactions and exchange [9], and their motion and energies can be expected to be affected when the interplanar stacking is changed in the sliding LP-to-HP-I transition. With the clusters now positioned vertically above each other in the high-pressure

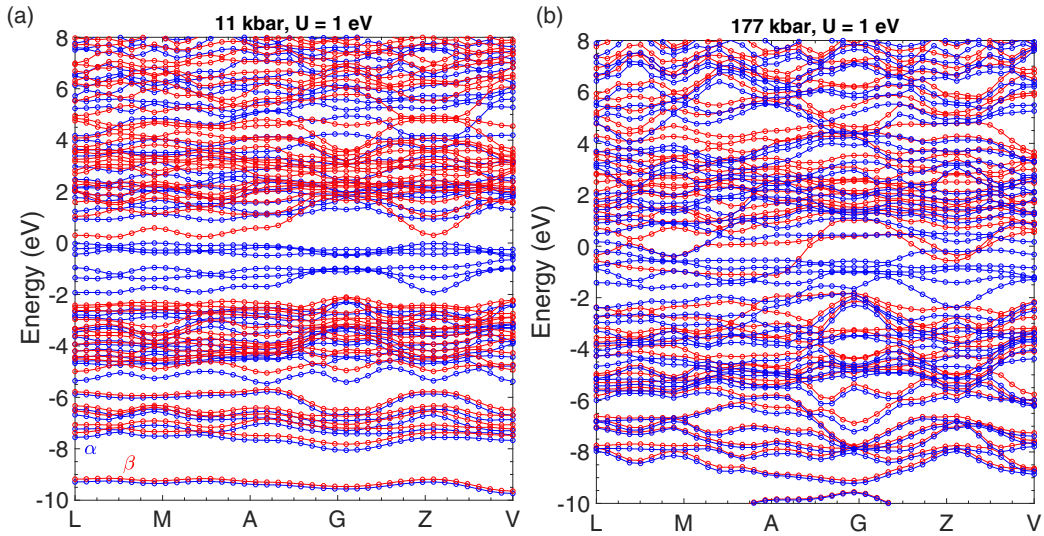

FIG. 8. Calculated spin-polarized band structures (up spin states in blue and down spin states in red) of $V_{0.9}PS_3$ with a Hubbard U of 1 eV (a) at 11 kbar (band gap of 0.226 eV) and (b) at 177 kbar.

phase, it is reasonable that such vibrational modes either change in energy or are made extinct through this structural transition.

As a complement to the Raman study, we were also able to calculate the band structures and density of states for $V_{0.9}PS_3$ in both the LP and the HP-I structural phases. This represents the first such calculation, informed by detailed high-precision experimental structural results, in the MPS_3 family, which again share the same structures and pressure-driven structural transitions. As with previous works, the band structure appears metallic until an on-site Coulomb interaction in the form of a Hubbard U is included in the calculation. U has the effect of splitting the states at the Fermi level and hence recovering the insulating or semiconducting behavior seen in experiments across the MPS_3 compounds. This behavior, along with the presence of magnetic order, forms a smoking gun for a Mott insulator and correlated electron physics—along with the observation of pressure continuously closing the band gap. The exact choice of U value, as always with this kind of calculation, has a strong effect on the size of the band gap obtained. This is particularly problematic in the case of $V_{0.9}PS_3$, which does not obey Arrhenius-type thermally activated transport and so does not allow a simple extraction of a meaningful band gap from the resistivity. Figure 6 shows the calculated spin-polarized densities of states for the s, p, and d bands, and their sum, in the low-pressure insulating phase and in the high-pressure metallic phase. This calculation used a U value of 3 eV, within the range 3.0–3.5 eV [45–47] commonly used for vanadium ions, and results in a low-pressure band gap of around 1.5 eV. This gap was found to decrease by around 0.5 eV per eV of U reduced in a linear fashion. At U values above 3.5 eV the 177-kbar high-pressure data also develop a band gap, in contradiction to experiments, placing an upper bound on the choice of value. The full spin-polarized band structure plots for the low- and high-pressure phases are shown in Fig. 7. The reported band-gap size estimated in the literature is around 0.25 eV [12,32,33], but again this value is not strictly physical and further spectroscopic study is needed to clarify the electronic structure of even ambient-pressure $V_{0.9}PS_3$. A gap of 0.25 eV can be achieved through a (perhaps unphysically low) U of 1 eV, as shown in Fig. 8 for completeness.

IV. DISCUSSION

We have reported the first high-pressure Raman spectroscopy study into the MPS_3 family of materials, a new family of 2D compounds with rich potential, along with the first precise calculations of electronic band structures and vibration modes, informed by our earlier high-precision structural data at high pressures. The Raman peaks observed in room-temperature powder $V_{0.9}PS_3$ all shift linearly upwards in energy as the pressure is increased, except for the p2 peak, which exhibits a kink or stiffening change of gradient at a pressure of 120 kbar, where an isostructural Mott insulator–metal transition was previously seen. This peak uniquely corresponds to out-of-plane ionic motion and so its stiffening can be considered a sign of the system becoming more 3D and exhibiting interplanar interactions at the transition. Between 20 and 80 kbar, $V_{0.9}PS_3$ undergoes a gradual structural transition from the LP to the HP-I phase (these phases are universal across all studied MPS_3). Over this range peak p3 was seen to be gradually suppressed and then to disappear at the point corresponding to LP phase extinction.

Theoretical *ab initio* calculations were able to reproduce well the Raman spectra and allow mapping of the individual peaks, and the band structures and densities of states for each phase were established. These are sensitive to the choice of Hubbard U parameter, and more work remains to be done via spectroscopy or photoemission techniques to probe the details of the band structure experimentally, but the calculations were able to produce results agreeing well with the experimental observations. The opening-up of a narrow band gap, via the tuning of an on-site Coulomb U, and then its subsequent gradual closing with pressure form key evidence for correlated physics and the Mott insulating state in this exotic and truly 2D compound.

ACKNOWLEDGMENTS

The authors would like to thank Kaixuan Zhang, Inho Hwang, Junghyun Kim, Nahyun Lee, and Siddharth Saxena for their generous help and discussions. This work was supported by the Institute for Basic Science (IBS) in Korea (Grant No. IBS-R009-G1), KOPRI, Korea (Grant No. PE19200), and the NRF, Korea (Grant No. 2017R1A2A1A17069511).

[1] J.-G. Park, J. Phys.: Condens. Matter **28**, 301001 (2016).
[2] P. Ajayan and K. Banerjee, Phys. Today **69**, 38 (2016).
[3] N. Samarth, Nature **546**, 216 (2017).
[4] Y. Zhou, H. Lu, X. Zu and F. Gao, Sci. Rep. **6**, 19407 (2016).
[5] K. S. Burch, D. Mandrus, and J.-G. Park, Nature **563**, 47 (2018).
[6] W. Klingen, G. Eulenberger, and H. Hahn, Naturwissenschaften **55**, 229 (1968).
[7] W. Klingen, G. Eulenberger, and H. Hahn, Naturwissenschaften **57**, 88 (1970).
[8] W. Klingen, R. Ott, and H. Hahn, Z. Anorg. Allg. Chem. **396**, 271 (1973).
[9] V. Grasso and L. Silipigni, Riv. Nuovo Cimento **25**, 1 (2002).
[10] R. Brec, D. M. Schleich, G. Ouvrard, A. Louisy, and J. Rouxel, Inorg. Chem. **18**, 1814 (1979).
[11] G. Ouvrard, R. Brec, and J. Rouxel, Mater. Res. Bull. **20**, 1181 (1985).
[12] G. Ouvrard, R. Fréour, R. Brec, and J. Rouxel, Mater. Res. Bull. **20**, 1053 (1985).
[13] R. Brec, Solid State Ion. **22**, 3 (1986).
[14] J. U. Lee, S. M. Lee, J. H. Ryoo, S. M. Kang, T. Y. Kim, P. W. Kim, C. H. Park, J.-G. Park, and H. S. Cheong, Nano Lett. **16**, 7433 (2016).
[15] C. T. Kuo, M. Neumann, K. Balamurugan, H. J. Park, S. Kang, H. W. Shiu, J. H. Kang, B. H. Hong, M. S. Han, T. W. Noh, and J.-G. Park, Sci. Rep. **6**, 20904 (2016).

[16] K. Kurosawa, S. Saito, and Y. Yamaguchi, J. Phys. Soc. Jpn. **52**, 3919 (1983).
[17] K. Okuda, K. Kurosawa, S. Saito, M. Honda, Z. Yu, and M. Date, J. Phys. Soc. Jpn. **55**, 4456 (1986).
[18] A. R. Wildes, S. J. Kennedy, and T. J. Hicks, J. Phys.: Condens. Matter **6**, L335 (1994).
[19] A. R. Wildes, B. Roessli, B. Lebech, and K. W. Godfrey, J. Phys.: Condens. Matter **10**, 6417 (1998).
[20] K. C. Rule, G. J. McIntyre, S. J. Kennedy, and T. J. Hicks, Phys. Rev. B **76**, 134402 (2007).
[21] A. R. Wildes, H. M. Rønnow, B. Roessli, M. J. Harris, and K. W. Godfrey, J. Magn. Magn. Mater. **310**, 1221 (2007).
[22] A. R. Wildes, K. C. Rule, R. I. Bewley, M. Enderle, and T. J. Hicks, J. Phys.: Condens. Matter **24**, 416004 (2012).
[23] A. R. Wildes, V. Simonet, E. Ressouche, G. J. McIntyre, M. Avdeev, E. Suard, S. A. J. Kimber, D. Lançon, G. Pepe, B. Moubaraki, and T. J. Hicks, Phys. Rev. B **92**, 224408 (2015).
[24] A. R. Wildes, V. Simonet, E. Ressouche, R. Ballou, and G. J. McIntyre, J. Phys.: Condens. Matter **29**, 455801 (2017).
[25] D. Lançon, H. C. Walker, E. Ressouche, B. Ouladdiaf, K. C. Rule, G. J. McIntyre, T. J. Hicks, H. M. Rønnow, and A. R. Wildes, Phys. Rev. B **94**, 214407 (2016).
[26] C. R. S. Haines, M. J. Coak, A. R. Wildes, G. I. Lampronti, C. Liu, P. Nahai-Williamson, H. Hamidov, D. Daisenberger, and S. S. Saxena, Phys. Rev. Lett. **121**, 266801 (2018).
[27] M. J. Coak, S. Son, D. Daisenberger, H. Hamidov, C. R. S. Haines, P. L. Alireza, A. R. Wildes, C. Liu, S. S. Saxena, and J.-G. Park, arXiv:1903.10971 [NPJ Quantum Mater. (to be published)].
[28] Y. Wang, Z. Zhou, T. Wen, Y. Zhou, N. Li, F. Han, Y. Xiao, P. Chow, J. Sun, M. Pravica, A. L. Cornelius, W. Yang, and Y. Zhao, J. Am. Chem. Soc. **138**, 15751 (2016).
[29] M. Tsurubayashi, K. Kodama, M. Kano, K. Ishigaki, Y. Uwatoko, T. Watanabe, K. Takase, and Y. Takano, AIP Adv. **8**, 101307 (2018).
[30] Y. Wang, J. Ying, Z. Zhou, J. Sun, T. Wen, Y. Zhou, N. Li, Q. Zhang, F. Han, Y. Xiao, P. Chow, W. Yang, V. V. Struzhkin, Y. Zhao, and H.-K. Mao, Nat. Commun. **9**, 1914 (2018).
[31] B. L. Chittari, Y. Park, D. Lee, M. Han, A. H. MacDonald, E. Hwang, and J. Jung, Phys. Rev. B **94**, 184428 (2016).
[32] R. Brec and J. Rouxel, in *New Ways to Save Energy* (Springer, Berlin, 1980), p. 620.
[33] K. Ichimura and M. Sano, Synth. Met. **45**, 203 (1991).
[34] S. Lee, P. Colombet, G. Ouvrard, and R. Brec, Mater. Res. Bull. **21**, 917 (1986).
[35] D. J. Dunstan and I. L. Spain, J. Phys. E **22**, 913 (1989).
[36] I. L. Spain and D. J. Dunstan, J. Phys. E **22**, 923 (1989).
[37] H. K. Mao, J. Xu, and P. M. Bell, J. Geophys. Res. **91**, 4673 (1986).
[38] S. J. Clark, M. D. Segall, C. J. Pickard, P. J. Hasnip, M. I. J. Probert, K. Refson, and M. C. Payne, Z. Kristallogr. Cryst. Mater. **220**, 567 (2005).
[39] J. P. Perdew, K. Burke, and M. Ernzerhof, Phys. Rev. Lett. **77**, 3865 (1996).
[40] A. Tkatchenko and M. Scheffler, Phys. Rev. Lett. **102**, 073005 (2009).
[41] J. D. Head and M. C. Zerner, Chem. Phys. Lett. **122**, 264 (1985).
[42] S. Baroni, S. de Gironcoli, A. Dal Corso, and P. Giannozzi, Rev. Mod. Phys. **73**, 515 (2001).
[43] D. Porezag and M. R. Pederson, Phys. Rev. B **54**, 7830 (1996).
[44] B. Himmetoglu, A. Floris, S. de Gironcoli, and M. Cococcioni, Int. J. Quantum Chem. **114**, 14 (2013).
[45] B. Himmetoglu, A. Floris, S. de Gironcoli, and M. Cococcioni, Phys. Rev. B **73**, 195107 (2006).
[46] F. Aryasetiawan, K. Karlsson, O. Jepsen, and U. Schönberger, Phys. Rev. B **74**, 125106 (2006).
[47] S. Lutfalla, V. Shapovalov, and A. T. Bell, J. Chem. Theory Comput. **7**, 2218 (2011).
[48] A. Jovanović, A. S. Dobrota, L. D. Rafailović, S. V. Mentus, I. A. Pašti, B. Johansson, and N. V. Skorodumova, Phys. Chem. Chem. Phys. **20**, 13934 (2018).
[49] I. Kylänpää, J. Balachandran, P. Ganesh, O. Heinonen, P. R. C. Kent, and J. T. Krogel, Phys. Rev. Mater. **1**, 065408 (2017).